Fragmentation of 1.2 GeV per nucleon ^{139}La

W. B. Christie,* J. L. Romero, F. P. Brady, C. E. Tull,† G. P. Grim, B. McEachern, and J. C. Young‡
Department of Physics, University of California at Davis, Davis, California 95616

H. J. Crawford,§ D. E. Greiner, P. J. Lindstrom, and H. Sann‖
Lawrence Berkeley Laboratory, University of California at Berkeley, Berkeley, California 94720

U. Lynen
Gesellschaft für Schwerionenforschung, D-64220 Darmstadt, Federal Republic of Germany
(Received 28 June 1993)

The fragmentation of 1.2 GeV per nucleon ^{139}La nuclei has been studied. Total charge changing cross sections for H (CH_2-C), C, and Pb target nuclei, and elemental production cross sections for C and CH_2 targets for $1 \leq \Delta Z \leq 30$ have been measured. For heavy projectile fragments, the projected transverse momenta extracted are generally larger than predicted by models based on the internal momenta of nucleons in nuclei. Fits to the heavy fragment momentum distributions yield additional transverse momenta or "bounce-off" which range from $\simeq 500$ to 1000 MeV/c.

PACS number(s): 25.70.Mn

I. INTRODUCTION

The fragmentation of relativistic nuclei has been studied in recent years as beams up to $\simeq 1-2$ GeV/nucleon became available from the Bevalac at Lawrence Berkeley Laboratory and more recently from SIS at GSI, Darmstadt. Some of the salient features were established in the early pioneering work with beams of light projectile nuclei [1–6]: The projectile fragments produced tend to maintain the beam velocity with only small mean downshifts in velocity (or momentum per nucleon). Except for proton "fragments" (and allowing for the very small downshift) the measured momentum distributions in the projectile frame are nearly Gaussian and isotropic, and relatively independent of beam energy. Within experimental uncertainties, the momentum widths are target independent and, at least up to $A_B=40$, their dependence on fragment mass (A_F) and beam projectile mass (A_B) are explained largely by the internal momenta of nucleons in the beam nuclei. Predictions of these widths differ somewhat depending on whether one assumes a completely uncorrelated (Fermi gas) model [7] or a correlated nucleon shell model [8] with complete (angular momentum) pairing of the nucleons. The projectile fragmentation of relativistic ^{16}O and ^{12}C produce longitudinal (p_z) data [2] which tend to favor the smaller momentum widths of the correlated model [8].

The fragment production cross sections are nearly energy independent and (at least) by 1 GeV per nucleon appear to have reached limiting fragmentation and factorization. In the case of beam projectile B incident on target T, factorization (in its strongest form) implies that the production cross section for fragment F in $B+T \rightarrow F+$ anything, can be written as $\sigma_{BT}^F=\gamma_T\gamma_B^F$, so that different targets change the magnitude of all the production cross sections in the same way [1]. The data of Lindstrom *et al.* [3] for ^{16}O and ^{12}C fragmentation on a large range of nuclei (H→Pb) indicate (after correcting for Coulomb dissociation) that γ_T is proportional to $A^{1/4}$ or to $A^{1/3}+$const, thus implying the largely peripheral nature of the interaction producing fragmentation. In a more recent analysis of these data (and also that for ^{56}Fe projectiles) Olson *et al.* [9] distinguish strong (above) and weak ($\sigma_{BT}^F=\gamma_{BT}\gamma_B^F$) factorization, and find that strong factorization holds better than predicted by the abrasion-ablation and by the (projectile) excitation-decay fragmentation models. Electromagnetic dissociation of 1.7 GeV per nucleon ^{18}O projectiles has also been studied by Olson *et al.* [10].

As they became available, the fragmentation of heavier beams was investigated. The data of Viyogi *et al.* [11] for 213 A MeV ^{40}Ar fragmentation by carbon also showed Gaussian distributions for the longitudinal component of momentum for a wide range of projectile fragments. In the Goldhaber model [7], where the projectile frame x, y, and z momentum component widths are characterized by $\sigma^2=\sigma_0^2 A_F(A_B-A_F)/(A_B-1)$, the data indicate a mean value of σ_0(expt)=94 MeV/c for the longitudinal (beam direction) momentum widths. In this model σ_0 is related to the Fermi momentum via $\sigma_0^2=p_F^2/5$. Thus, the above σ_0(expt) yields $p_F=209\pm11$ MeV/c which can be com-

*Current address: Lawrence Berkeley Laboratory, Berkeley, CA 94720.
†Current address: Louisiana State University, Baton Rouge, LA 70803.
‡Permanent address: California State University at Chico, Chico, CA 95929.
§Also at Space Science Laboratory, LBL.
‖Permanent address: GSI, Darmstadt, FRG.

pared to the value 251±5 MeV/c derived from electron scattering on ^{40}Ca [12]. The data favor a smaller momentum width than that predicted by the (uncorrelated) Fermi-gas model. (For ^{12}C and ^{16}O the fragmentation measurements [2], using the Goldhaber [7] model, yield experimental values of $p_F = 144$ and 171 MeV/c respectively, while the electron-scattering data values are 221 and 230 MeV/c, respectively.) The measured cross sections for fragment isotopic distributions are also nearly Gaussian and can be well described within the framework of the abrasion-ablation models [13-16], but, apparently not as well by thermal equilibrium models [7,2] wherein the thermal decay of the excited *projectile* governs the distribution of nuclei which result.

The fragmentation of 1.88A GeV ^{56}Fe by a range of targets (H→Pb) has been studied by Westfall *et al.* [17]. Elemental production cross sections $\sigma(Z)$ were measured for $Z = 13-25$. Strong factorization is observed to hold for the nuclear part of the fragment production cross sections, and the target factor can be parametrized as $\gamma_T = aA_T^d$ or $\gamma_T = c(A_T^{1/3} + A_B^{1/3} - b)$ with $d \simeq 0.18$ and $b = 1.2$ fm. Enhancement of one proton removal by heavy targets is explained by Coulomb excitation as in the case of lighter projectile data [18].

In analyzing the fragmentation of ^{56}Fe projectiles Oliveira *et al.* [16] found that an additional frictional or final-state interaction energy had to be added to the abrasion fragment (or prefragment) with the result that the final fragment isotopic distributions predicted after the ablation stage were in much better agreement with the data. In their model this excitation energy comes from participant nucleons recoiling into the spectator prefragments. Recently, Gaimard and Schmidt [19] have proposed calculating this energy in terms of nucleon hole states produced in the abrasion fragment when nucleons are removed by the abrasion process. They estimate this to be ≃13–15 MeV per nucleon removed from the projectile.

Binns *et al.* [20] have studied the fragmentation of relativistic ^{139}La and ^{197}Au beams on targets of polyethylene, carbon, aluminum, and copper. Attention was focused on fragments whose atomic numbers were only changed by +1, −1, −2, or −3 units ($\Delta Z = +1$ to −3). It was found that the $\Delta Z = +1$ cross section is ≃10% of that for $\Delta Z = -1$ and about 1% of the total charge changing cross section. A striking feature is the large number of neutrons which are lost when only one, two, or three protons are lost by the projectile. For ^{139}La projectiles at ≃515, 618, and 775 MeV per nucleon they [20] found the medium mass loss to be given by $\Delta A \simeq -10$, −10, and −12 units when $\Delta Z = -1$. There is little target dependence. When $\Delta Z = -2$, $\Delta A \simeq -15$, −14, and −15, and when $\Delta Z = -3$, $\Delta A \simeq -20$, −18.5, and −19.5 units at the above energies. For ^{197}Au projectiles, the ΔA values are larger: $\Delta A \simeq -12.5$, −12.5, and −14.5 for $\Delta Z = -1$ at the three energies. These large neutron losses are difficult to explain in the standard abrasion-ablation model [13] or in the model of Silverberg and Tsao [21]. The surface energies calculated in the clean-cut abrasion-ablation (AA) model are too small to allow ≃10 neutrons to evaporate. Additional "frictional" energy such as that introduced by Oliveira *et al.* [16] or particle-hole energy as used by Gaimard and Schmidt [19] appears to be required.

In an earlier work Binns *et al.* [22] measured the total and partial charge changing cross sections for ^{84}Kr, ^{132}Xe, ^{165}Ho, and ^{197}Au beams of 1.68, 1.49, 1.13, and 1.05 GeV per nucleon, respectively, incident on targets of Al, C, and CH_2. More recently, Cummings *et al.* [23] extended these measurements to a wider energy range, and to Cu and Pb targets. They also parametrized the variation of the elemental cross sections as a function of energy, projectile, target, and fragment [24]. Also from the Bevalac facility, Webber, Kish, and Schrier [25] have produced an extensive and systematic study of total, elemental, and isotopic cross sections for beams of nuclei from ^{12}C to ^{58}Ni incident on targets of hydrogen, helium, and carbon at energies from 300 to 1700 MeV per nucleon. They also provide comprehensive comparisons with, and references to, other data.

In the present experiment only the charge, Z_F, and vertical deflection of medium and heavy beam rapidity fragments were measured using MUSIC I [26]. Earlier [27,28], based on preliminary analyses of these data, we reported the observation of transverse momenta of fragments which were larger than predicted by models such as that of Goldhaber [7]. This was the first direct evidence of bounce-off of the heavy fragments.

II. EXPERIMENT AND DATA

The beam of ^{139} La nuclei at ≃1.3 GeV per nucleon was produced by the Bevalac at Lawrence Berkeley Laboratory. The fragmentation of these beam projectiles by C, CH_2, and Pb nuclei took place at a mean energy near 1.2A GeV. The measurements were made at the HISS (Heavy-Ion Superconducting Spectrometer) facility [29] with MUSIC, a multiple-sampling ionization chamber [26], which is a component of the HISS system at the Bevalac. The experimental arrangement, shown in Fig. 1, is detailed in Ref. [26]. Very briefly, a collimating veto, a beam monitor, and the target were placed near the center of the HISS dipole (whose field was turned off). After passing through these, the beam and fragments traveled 7.8 m and passed through MUSIC.

MUSIC has an active volume 2 m wide×1 m high×1.5 m deep along the beam direction, and uses time-projection-chamber principles and electronics. At the top is a cathode plane at negative high voltage of ≃21 kV. Ionization tracks are drifted (down) through a

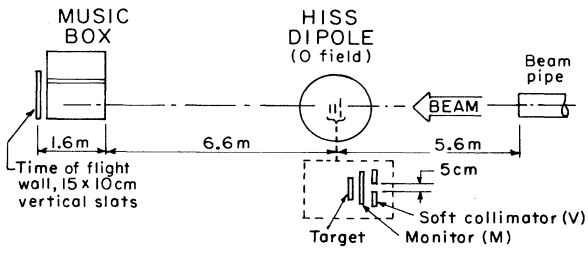

FIG. 1. The experimental setup at the Bevalac HISS facility for the 1.3 GeV/nucleon ^{139}La run.

grounded Frisch grid to the positive potential ($\simeq$800 V) anode plane which, for these measurements, was divided into left and right halves as seen by the beam. This increases the multiplicity capability in the horizontal plane. Each half is segmented along the ion tracks into 60 2- and 4 6-cm-thick anode cells. Thus, 64 spatial samples of ionization are collected every 100 ns to obtain 64 vertical profiles of the chamber charge distribution. The 64 samples provide a track energy-loss distribution whose average measures the mean energy deposited (which depends on the fragment velocity and on the charge as Z_f^2), as well as (from drift time) 64 vertical (or x) positions of the track.

We used P-10 (90% Ar, 10% CH_4) as the counting gas in MUSIC and during this run measured a drift velocity of 5.3×10^6 cm/s at $E/P=0.28$ V/cm Torr which agrees with quoted values. The field cage of MUSIC is contained in a stainless-steel cylindrical tank 2.2 m long and 2.8 m inside diameter. Thin gas (double) windows cover the ends of the tank, and during operation argon gas is flowed through the 1.5 cm gap in the double windows. This helps keep the gas free of contaminants such as oxygen which can give rise to large electron attachment loses. In addition, removable iron end caps can be placed over the gas windows and the tank evacuated and outgased (so to reduce gas impurities) prior to flushing and filling with the counting gas. We observe electron losses of about 0.1%/cm. Before a data run the chamber is evacuated and purged three or four times. During the run six standard cubic feet per hour of P-10 are flowed through the chamber, and one to two standard cubic ft/h of Ar through each double window gap.

The detector uses electronics which were developed for the time projection chamber (TPC) [30,31]. After an ion passes through the chamber the resulting electron cloud drifts down towards the Frisch grid and anode plane at about 0.5 cm/100 ns. The induced charge on each anode is sensed by a low noise, charge-sensitive preamplifier which is attached to the outside of the tank. From the preamp the signal travels through about 20 m of coaxial ribbon cable into a shaping amplifier designed to output a pseudo-Gaussian pulse which peaks in about 250 ns. The signal then enters a charge-coupled device (CCD) which samples the output of the amplifier every 100 ns (10 MHz). Assuming that the ionizing particle triggered the electronics, the CCD will collect a preselected number of samples of the analog signal, each sample denoted by a "bucket" number. When the CCD has collected the samples it is ready to be read. The digitized output is stored in a RAM buffer located in the MUSIC CAMAC controller module. A microprogramed branch driver (MBD) reads the event from the CAMAC module memory and sends it through the PDP 11/45 to tape and a shared disk which is also addressable by a VAX. More details of the electronics and data acquisition are given in Ref. [26].

When an ion such as a nuclear fragment passes through MUSIC it loses energy primarily through interactions with the electrons in the gas. The distribution function for the energy lost by the incident particle depends upon the particle's velocity and charge, and on the ratio of the mean energy loss, Δ, over the path length to the maximum energy ϵ_{max}, which can be imparted to one electron in a collision. This ratio is denoted by $\chi=\Delta/\epsilon_{max}$. As the ratio $\chi\rightarrow0$, the energy lost in individual collisions becomes important and the energy-loss distribution function becomes wide and asymmetric with a high-energy tail. This is the Landau limit [32]. For large values of χ the incident particle makes many collisions with the electrons and the energy-loss distribution function becomes Gaussian. Vavilov [33] solved the problem of energy loss by charged particles. His distribution function goes to the Landau limit for $\chi\rightarrow0$, goes to the Gaussian limit for $\chi\gg1$, and covers the region between the two limits.

While the Vavilov distribution correctly gives the energy-*loss* distribution it does not give the distribution observed with MUSIC, which is the energy *deposited* in the anode cells. The reason for this difference is that the high-energy, knock-on electrons resulting from collisions with the incident particle have a practical range larger than the thickness of the anode cell (and of MUSIC), and escape from the cell without depositing all their energy. Calculations for energy deposited in an absorber have been made by Badhwar [34] and Adams *et al.* [35], and these fit the single-cell resolutions that we measure for Ar and La very well [26]. For the 2-cm cells used here the measured (nearly Gaussian) single-cell resolution was (4.7$\pm$0.3)%, while the prediction of the Badhwar theory is 4.5% and that of Vavilov 16.9% full width at half maximum (FWHM) [26].

For each anode the time distribution of analogue-to-digital converter (ADC) values (of charge) for a single track has roughly a Gaussian distribution above some offset. In our analysis of the single-cell resolutions as well as for track (whole chamber) average resolutions we used the peak or largest (time bucket) ADC instead of time integrating each pulse. We have checked that the two methods give the same results. This is expected since the pulse rise times are nearly constant and hence the peak ADC is directly proportional to the current induced between the Frisch grid and the anode plane.

The width of the ($\simeq$ Gaussian) time distributions is $\simeq$600 ns or 3 cm (FWHM). By fitting one can find the centroid to within $\simeq$2 mm and by averaging over n cells get within $\simeq2$ mm/$\sqrt{n}$. For $n=64$ this is 250 μm or a one-standard-deviation (SD) uncertainty in vertical height of $\sigma_x\simeq100$ μm. This good position resolution for heavily ionizing particles has been confirmed in the tests of the new three coordinate MUSIC called MUSIC II [36] which is used for momentum analysis tracking and charge measurement of $Z\gtrsim5$ fragments at HISS. We used this good position resolution to measure the vertical deflection (top of Fig. 2) of fragments and to check that the angle of the fragments pointed back to the beam-on target area. In Fig. 2 (top) the drift time is plotted against fragment charge for a 1.3A GeV La beam incident on a 2.68-g/cm^2 carbon target. Since energy loss is proportional to Z^2, the measured single-cell resolution, (4.7$\pm$0.3)% FWHM, translates into 2.35% resolution in charge (assuming zero velocity dispersion). For n cells the resolution should improve by $1/\sqrt{n}$. We used 54 2-cm cells and thus expect a 54-cell track average energy

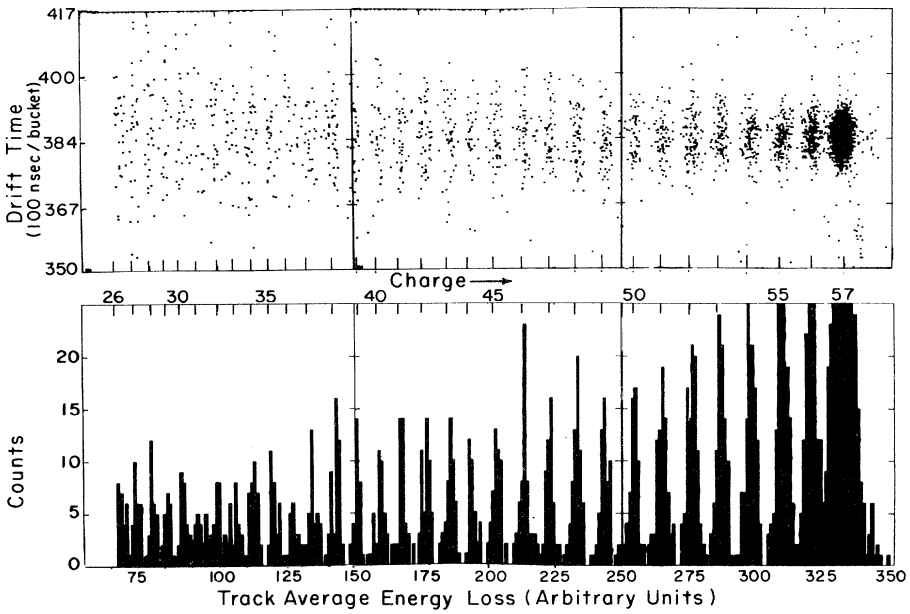

FIG. 2. Analyzed data from MUSIC. Top: Drift time vs track average energy loss and charge of fragments from ^{139}La (1.2 GeV/nucleon)+C. Bottom: Projected charge spectrum.

resolution of $\simeq 0.64\%$ and a charge resolution of 0.32%. With a 2.68-g/cm^2 carbon target we observe 1.06% (FWHM) energy resolution. This corresponds to a ΔZ (FWHM) of 0.30 charge units for La($Z=57$). The energy and charge resolution are larger than the expected value; ΔZ(expected)$=0.18$ charge units. We believe the difference between the observed and predicted could be due to velocity dispersion in the beam, plus that due to target and other energy losses.

The bottom half of Fig. 2 shows the 54-cell track average energy loss, time-projected spectrum. Charge is indicated above the energy-loss peaks. Above a charge threshold of $Z_F=10$, most ($\simeq 95\%$) of the events are single tracks. Data such as these were also taken for target out, a CH_2 target of 2.09 g/cm^2, a second carbon target of 5.56 g/cm^2, and a lead target of 3.93 g/cm^2.

III. ANALYSIS AND DISCUSSION

A. Cross sections

The total charge changing cross sections give a measure of the probability of the beam particles, $^{139}_{57}$La nuclei, have a charge other than $Z=57$ after traversing a target. In general, the total cross section, σ, is related to the transmitted intensity, I, the number, n, of target nuclei per cm^2 and the incident intensity, I_0 by $I=I_0\exp(-n\sigma)$, the well-known collimated beam attenuation equation. The incident flux I_0 is determined by the scintillator S_1, just upstream from the target. The S_1 threshold is set to include $Z=57$, but to exclude to a great extent $Z<57$. The transmitted flux of nuclei, $I(Z)$, with different charges, Z, is measured by MUSIC down to $Z=26$. Target-out runs were made to measure the beam attenuation, due mainly to the air path and the chamber windows, and to measure the production of fragments with charges other than the beam charge by the air and windows.

The total charge changing cross sections are obtained directly after the target-out corrections are made. Table I summarizes the results for the three nuclei. For the Pb target only a small sample of data was collected resulting in the large uncertainty.

A comparison of the data with the models can be made. The models give total reaction cross sections or empirical charge changing formulas. In the former case the removal of only neutrons (which we do not measure) is included, so one expects the data to fall below the predictions. One model is the simple, geometric, hard-sphere model which is based on the notion that if the im-

TABLE I. Our measured total charge changing cross sections (b) compared to model predictions (see text).

Target	$\sigma\lvert\Delta Z\rvert\geq 1$ (This expt.)	$\pi(R_T+R_B-2\Delta R)^2$ (Bradt-Peters)	$\pi(R_T+R_B)^2$ (Hard sphere)	$\pi(R_T+R_B-b)^2$ (Westfall)	σ_R (Karol)
H	1.44±0.15	1.50	1.73	1.32±0.06 ($A_T=0.089$)	1.4
^{nat}C	2.13±0.10	2.25	2.52	2.52±0.1	2.8
^{nat}Pb	4.4±3.1	5.17	5.58	6.04±0.15	6.6

pact parameter is less than or equal to the sum of the radii of the projectile and target an interaction will take place. The total reaction cross section is then $\sigma_R = \pi r_0^2 (A_T^{1/3} + A_B^{1/3})^2$. For $r_0 = 1.2$ fm, Table I (column four) gives these predictions of σ_R. It can be seen that the measured values (column two) are 17, 15, and 21% below the predicted values for hydrogen, carbon, and lead, respectively. This trend could reflect the effects of nuclear transparency as well as the fact that we do not measure neutron-only removal. (The latter is estimated later.)

A comparison can also be made with the overlap model of Bradt and Peters [37] which was first devised to explain early cosmic-ray data. This model has an overlap parameter, ΔR, to allow for some surface transparency and predicts $\sigma_R = \pi (R_T + R_B - 2\Delta R)^2$. Here we use the parameters of Cleghorn *et al.* [38] who found $r_0 = 1.2$ fm and $\Delta R = 0.25$ fm. The resulting predictions are given in the third column of Table I. Our observed values are 4, 5, and 15% below these predictions for H, C, and Pb, respectively.

Westfall *et al.* [17] measured charge changing cross sections with 1.88 GeV/nucleon ^{56}Fe nuclei incident on a range of targets H to U. They fit a Bradt-Peters form

$$\sigma(\Delta Z \geq 1) = \pi r_0^2 (A_T^{1/3} + A_B^{1/3} - b)^2 ,$$

and found best-fit parameters for $r_0 = 1.35$ and $b = 0.83 \pm 0.12$ fm. They also found that in order to have the H cross section lie on this line they had to use $A_T = 0.089$ in the above equation. In Table I (column five) the predictions of Westfall *et al.* for $\sigma(\Delta Z \geq 1)$ are shown. Our measurements are 9% higher, 15% lower, and 27% lower for H, C, and Pb, respectively.

A more recent model is that of Karol [39] (sometimes referred to as a soft-sphere model). It is based on the (semiclassical) optical model, and uses tapered nuclear density distributions and experimental nucleon-nucleon cross sections. The predictions σ_R shown in Table I (last column) use experimental values for the half central density radius, the skin thickness, the rms radius, etc., where available. The hydrogen cross section is in good agreement while our carbon value is below that predicted. As above, this is in the direction expected.

It should be noted that one can use a model calculation to estimate the contribution of the $\Delta Z = 0$ reactions to the total reaction cross section. If we use the abrasion-ablation model of Gaimard and Schmidt [19] we calculate this contribution to be 19% of the total for our carbon target data. (This model includes additional particle-hole or frictional energy of $\simeq 15$ MeV per participant and accounts better for the large ablation-stage neutron losses mentioned earlier.) Thus, the corrected (measured) reaction cross section for carbon would be 2.63 ± 0.13 b, in reasonable agreement with the reaction cross sections of the hard-sphere model. The cross section is approximately 10% above the Bradt-Peters prediction if one uses their parameters, but it is in reasonable agreement if one chooses Westfall's fitted parameters.

Data such as that in Fig. 2 (bottom) allow one to calculate elemental production cross sections, $\sigma(Z)$. Corrections for multiple interactions in the target were applied to obtain thin-target, $\sigma(Z)$ values. These were carried out as follows: It was assumed that data collected while the target was in place were independent of the target position along the beam path, due to the similarity of the target and surrounding medium. Thus, for the purpose of calculations it was assumed that the target was directly in front of MUSIC. Based on this assumption, the equations used to calculate the fragmentation cross sections (analogous to those of Ref. [17]) were

$$N_j = N_j^T + N_j' + N_j^{\mathrm{BF}} + N_j^{\mathrm{SF}} , \tag{1}$$

$$N_j' = N_{0j} \exp\{-\sigma_j s\} , \tag{2}$$

$$N_j^{\mathrm{BF}} = \sum_{i=1}^{j-1} \sigma_{ij} N_{0i} \frac{(\exp\{-\sigma_j s\} - \exp\{-\sigma_i s\})}{\sigma_i - \sigma_j} , \tag{3}$$

$$N_j^{\mathrm{SF}} = \sum_{i=1}^{j-1} \left[\frac{\sigma_{0i}}{\sigma_0} N_{00} (1 - \exp\{-\sigma_0 s\}) - N_j^T \right] \frac{\sigma_{ij}}{\sigma_i} , \tag{4}$$

$$N_j^T = \sigma_{0j} N_{00} \frac{(\exp\{-\sigma_j s\} - \exp\{-\sigma_0 s\})}{\sigma_0 - \sigma_j} , \tag{5}$$

where the N's are defined as follows.

N_j (N_{0j}) is the total number of $Z = 57 - j$ fragments detected with the target in (out).

N_j^T is the contribution to N_j from primary fragmentation of La in the target. Since the target is thick, some of the fragments created are attenuated. This is corrected for in Eq. (5).

N_j' is the direct contribution to N_j from background in the beam, attenuated by the target.

N_j^{BF} and N_j^{SF} are the relatively small secondary contributions to N_j from background fragments (i.e., contamination) in the beam which fragment in the target and secondary fragmentation of the primary beam in the target, respectively.

N_j, N_j^T, N_j^{BF}, and N_j^{SF} are related to the partial and total charge changing cross sections through Eqs. (2)–(5).

In these equations s is the target thickness in atoms/cm^2, σ_j is the attenuation cross section out of the jth channel, and σ_{ij} is the attenuation cross sections from the ith to jth channel.

An iterative computer program was then written to extract the partial charge changing cross sections for La on carbon using the equation set (1)–(5) and the data binned according to charge. The extracted cross sections for the two carbon targets were averaged and the results are listed in column two of Table II. The associated uncertainties have been estimated from the statistical uncertainties in the raw data. The same iterative method was then applied to the CH_2 data and the hydrogen cross sections were obtained by using the subtraction $\sigma_H = \frac{1}{2}(3\langle \sigma_{CH_2} \rangle - \sigma_C)$, where $\langle \sigma_{CH_2} \rangle$ is the average σ per nucleus. Column 4 of Table II lists these results. The iterative corrections ranged from $(8 \pm 2)\%$ at $Z = 55$ to $(24 \pm 4)\%$ for $Z = 25$ and were nearly target independent. The Pb data for $\sigma(Z)$ were not reliable due to statistical uncertainties.

Figure 3 shows the elemental production cross sections plotted against charge removal, ΔZ, for $^{139}_{57}$La incident on $^{\mathrm{nat}}$C nuclei. Comparisons can be made with the better

statistics measurements for ^{132}Xe+C fragmentation at 1.2A GeV reported by Kertzman *et al.* [40] and Binns *et al.* [22] whose data are shown in Fig. 3 as the triangles. Agreement between data sets is good. The solid curve represents the result of an abrasion-ablation calculation using the program of Ref. [19]. These results are also tabulated in Table II, column 5. The abrasion stage is macroscopic and uses the equations presented in Ref. [41]. These equations, given originally by Swiatecki [42], have been smoothed in Ref. [19] to avoid a discontinuity and improve the accuracy in that region of the impact parameter. (The abrasion-ablation model is usually attributed to Bowman, Swiatecki, and Tsang [13]. However the model was apparently first formulated and used by Eisenberg [43] to analyze data on cosmic-ray interactions at altitude.) The ablation part of the program [19] is based on the elegant formulation of the statistical model proposed by Campi and Hüfner [44]. The initial evolution of the evaporation stage is described in a macroscopic way using a master equation which leads to a diffusion-type equation. Particle evaporation depends on level densities and effective penetrabilities. The data (Fig. 3) are reasonably well represented in the range where ΔZ is not too large (where the projectile target nucleus overlap is still incomplete). The bump predicted around $\Delta Z \simeq 24$ is where one has central collisions, and it is expected that multifragmentation will be important and will wash out such a structure in the data. The calculation is absolute and the total reaction cross section is assumed to be given by $\pi(R_B + R_T)^2$ with $R = r_0 A^{1/3}$ and $r_0 = 1.22$ fm.

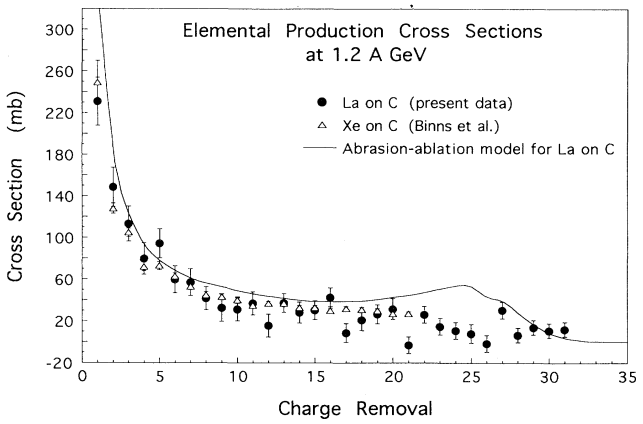

FIG. 3. The elemental production cross sections for $^{139}_{57}$La+C at 1.2 GeV/nucleon. The present data are compared to the data of Binns *et al.* (Ref. [20]) for ^{132}Xe+C at 1.2 GeV/nucleon and to abrasion-model calculations (see text). Note the cross section zero is raised.

TABLE II. Fragmentation cross sections in mb for La(1.2A GeV)+^{nat}C, $\langle CH_2 \rangle$, and H and abrasion-model calculations for La+C. $\langle CH_2 \rangle$ is the average cross section per nucleus in CH_2.

Frag. DZ	C	$\langle CH_2 \rangle$	H	Calculated C
1	231±24	212±23	203±37	389
2	148±19	163±20	170±32	185
3	113±17	113±17	113±28	123
4	80±15	98±16	108±25	93.8
5	94±14	99±15	101±24	78.2
6	60±13	81±15	92±23	68.7
7	57±13	55±14	55±22	61.3
8	42±11	74±13	89±20	56.3
9	33±12	21±12	15±20	52.9
10	31±11	38±12	42±19	49.1
11	37±11	32±12	29±18	46.1
12	16±11	9±11	5±17	43.8
13	37±9	39±10	41±15	41.9
14	28±10	20±10	16±16	40.0
15	30±9	36±10	39±16	39.0
16	40±9	24±9	16±14	38.8
17	9±8	5±8	3±13	38.7
18	21±9	14±9	11±15	39.2
19	27±9	19±9	16±15	40.6
20	31±10	−9±8	−29±12	42.7
21	−3±8	2±8	4±13	44.7
22	26±8	6±7	−5±11	47.4
23	15±8	−2±7	−11±11	50.8
24	11±8	−17±7	−31±11	53.8
25	8±9	6±8	5±13	53.2
26	−2±8	−12±7	−18±12	48.1
27	31±8	7±6	−4±10	39.4
28	7±7	−1±6	−5±10	28.1
29	14±7	18±7	20±12	17.1
30	11±7	−6±6	−15±10	8.8
31	12±8	13±7	13±12	3.9

From our data we also obtain an estimate of the $\Delta Z = +1$, or proton pickup, cross section. Our estimate is 19.4 mb for La on C with the statistical error of 23%. Since no target-out correction was made, this estimate is an upper limit. Binns *et al.* [20] obtain 21.7±1.6 mb at 1165 MeV/nucleon.

B. Transverse momentum distributions

From the distribution of drift times a mean vertical position x can be calculated for each track. The mean drift time or x position is shown in Fig. 2, top, for a range of fragment charges. We can calculate the track angle from the sample of drift times (x values) for each track and verify that the (projected) ion track pointed back to the target beam elevation. From the angular distribution for each fragment charge, which is nearly Gaussian in shape, a standard deviation $\sigma(\theta_x)$ was extracted. Figure 4 shows the fragment $\sigma(\theta_x)$, plotted against the fragment charge for the thin carbon target. Values before and after corrections for multiple Coulomb scattering and beam angular dispersion are shown. These corrections were obtained from the beam projectile data.

Conversion of θ_x and $\sigma(\theta_x)$ to p_x and $\sigma(p_x)$ values requires several (reasonable) assumptions. We assume that the longitudinal momentum per nucleon (the velocity) along the beam direction is maintained (as has been observed in earlier studies and is supported by the observed energy loss distributions in MUSIC). In order to calculate p_x and to compare the $\sigma(p_x)$ of the momentum distributions with theoretical predictions we need to estimate the mass A_F just after the abrasion takes place (rather

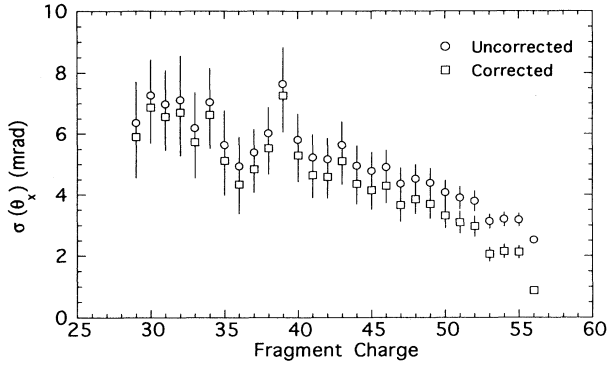

FIG. 4. The fragment angle distribution widths, $\sigma(\theta_x)[\equiv\theta_x(\text{rms})]$ vs fragment charge before and after corrections for multiple Coulomb scattering and beam angular dispersion.

than after the ablation stage which results in the detected fragment mass). The data of Binns *et al.* [20] and preliminary analyses of Müller [45] indicate that the charge change (ΔZ) during the ablation stage (following abrasion) is small for heavy fragment nuclei. Ablation (evaporation) calculations show, in agreement with Binns *et al.*, that the large Coulomb barrier ($\simeq$6–12 MeV) suppresses proton emission and that deexcitation is due predominantly to neutron emission. Thus (in the spirit of the fast, clean-cut abrasion-ablation model), we can use the detected fragment charge to estimate the abrasion mass, A_F, via $A_F = A_B Z_F / Z_B$. (For comparison, we also use for A_F the most stable mass for each measured Z_F.) Neglecting ablation stage effects, p_x is given by $p_x = \theta_x p_0 A_F$, where p_0 is the beam momentum per nucleon. This simple model yields the values of $\sigma(p_x)$ shown in Fig. 5(a). (The p_x are projected values of p_T along the vertical direction as measured in MUSIC.) The uncertainties given contain contributions due to assignment of the abrasion fragment mass (2.5–7.5 %), electron drift velocity in MUSIC (4%), longitudinal velocity (0.8%), and statistics (6–16 %). Preliminary values [27] and these values [28] of $\sigma(p_x)$ were reported earlier.

There is an additional uncertainty in p_x due to the fact that the momentum is measured after the ablation stage and contains recoil effects due to the evaporation of (mainly) neutrons. We assume that on average n nucleons evaporate isotropically into 4π (into x, y, and z directions). However, there will be statistical fluctuations of the order of $\sqrt{n}/3$ for each direction. If each evaporated neutron has an average kinetic energy of twice the nuclear temperature or $\simeq$2 MeV, the corresponding momentum is $\simeq$87 MeV/c. Thus, the evaporation of n nucleons produces a p_x momentum distribution with an SD of $\sigma_e(p_x)\simeq\sqrt{n}/3$ 87 MeV/c, or $\simeq$170 MeV/c for $n=12$. This, added in quadrature with the abrasion momentum, would have a relatively small effect except for fragments with Z near Z (beam) whose $\sigma(p_x)$ values are relatively small. The values of $\sigma(p_x)$ after subtracting in quadrature $\sigma_e = 170$ MeV/c are shown in Fig. 5(a).

Comparisons of the corrected values for $\sigma(p_x)$ with predictions based on the models of Golhaber [7] (G) and Lepore and Riddell [8] (LR) are shown in Fig. 5(b). As noted in the Introduction, the former is based on an independent-particle (Fermi-gas) model in which the only correlation among the nucleons in the projectile and in the fragment nucleus is that given by conservation of momentum, and the latter model uses independent-particle shell-model wave functions whose main features are harmonic-oscillator Gaussian factors. In the Goldhaber model, dependence on the Fermi momentum is via $\sigma_0^2 = p_F^2/5$. Here the p_F of La is taken to be 250 MeV/c [12]. The LR $\sigma(p_j)$ values for La are 0.54 times those of Goldhaber. For both models the predicted $\sigma(p_x)$ [Fig. 5(b)] are smaller than those obtained from the measurements. A fit to our data, with $A_F = Z_F A_B / Z_B$ [solid line in Fig. 5(b)] with the Goldhaber form yields a mean $\bar{\sigma}_0 = 160\pm12$ MeV/c, as compared to $\sigma_0(\text{G}) = 112$ and $\sigma_0(\text{LR}) = 60.5$ MeV/c. The fit is systematically below the data at large A_F and above it at medium A_F, thus indicating a slight fragment mass dependence for σ_0. A thicker (5.56 g/cm^2) C target gave $\bar{\sigma}_0 = 166\pm13$ MeV/c, which indicates that the effect of multiple nuclear interactions is small.

Figure 6 shows, both for $A_F = A_B Z_F / Z_B$ and for most stable A_F, corrected values of σ_0 extracted from the

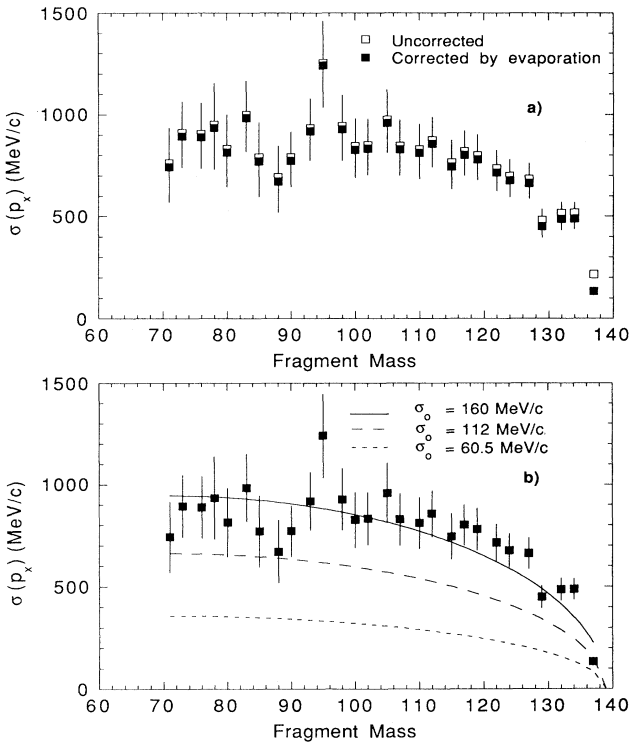

FIG. 5. (a) The fragment $\sigma(p_x)$ values derived from the data of Fig. 4 plotted against fragment mass. Also shown are the results of $\sigma(p_x)$ after applying a correction for neutron evaporation (see text). (b) Corrected $\sigma(p_x)$ are compared with the predictions of Golhaber ($\sigma_0 = 112$ MeV/c) and that based on the model of Lepore and Riddell ($\sigma_0 = 60.5$ MeV/c). The solid line corresponds to the best fit ($\sigma_0 = 160$ MeV/c). A_F (the abrasion mass) is assumed to be $A_B Z_F / Z_B$.

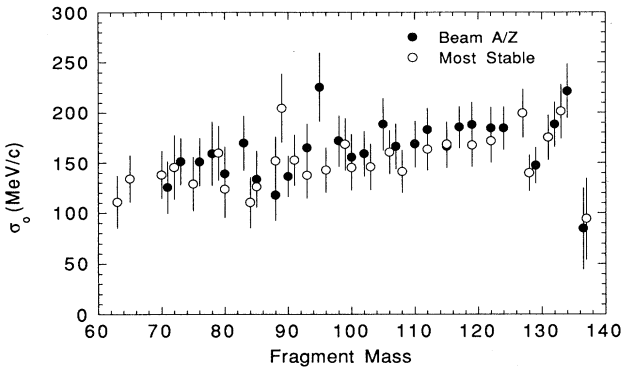

FIG. 6. Corrected values of σ_0(expt) (as defined by Goldhaber) plotted vs A_F (determined as described in the text).

^{139}La+^{nat}C data shown in Fig. 5. These σ_0 values depend on the value assumed for the mass A_F of the abrasion fragment. Thus, the σ_0 uncertainties reflect an estimated uncertainty in A_F of $\sigma(A_F)=1$ unit. As noted in the Introduction, the σ_0 values derived from the longitudinal momentum distributions for ^{12}C, ^{16}O, and ^{40}Ar fragmentation were less than the Goldhaber predictions ($\sigma_0^2=p_F^2/5$) by $\simeq$25–40%. Bertsch [46] argues that momentum anticorrelations of the nuclear shell model should suppress momentum fluctuations, and his calculations for p_Z are in agreement with the earlier ^{40}Ar fragmentation data [11]. In contrast with these earlier measurements, our transverse momentum distributions are about equal to or larger than these predicted from Goldhaber's model and may indicate additional (possibly collective) influences on p_T. This might also call into question an intrinsic feature of the model, namely, that the longitudinal and transverse momentum widths should be the same.

C. Transverse bounce

In order to explain the extra transverse momentum observed in the measured p_x momentum distributions we assume an additional transverse bounce $\mathbf{p}_B$. We fold p_B (bounce) with the Gaussian x-momentum distribution predicted by Goldhaber (σ_G) (or LR) and obtain the projected p_x distribution to compare to the data:

$$f(p_x,p_B,\phi)=Ce^{-(p_x-p_B\cos\phi)^2/2\sigma^2},$$

where ϕ is the angle $\mathbf{p}_B$ makes with the x axis. The above distribution includes the effects of multiple Coulomb scattering (MCS) and neutron evaporation, since it can be shown that the folding of Gaussians and Goldhaber momentum distributions can be included simply via the relation $\sigma^2=\sigma_G^2+\sigma_g^2$, where, in our case, $\sigma_g^2=\sigma_{MCS}^2+\sigma_e^2$ with $\sigma_e=170$ MeV/c.

The distribution $f(p_x,p_B,\phi)$ is integrated over the azimuth ϕ to yield the projected p_x distribution $f(p_x,p_B)$. The latter is compared to the measured p_x distribution, and a fit is obtained by varying p_B. To improve statistics we bin the data for a certain range of Z_F as shown below. We fix $\sigma_0=\sigma_0$(Goldhaber)=112 MeV/c and calculate $\sigma_{MCS}(Z)=\sigma_{MCS}(\text{beam})A_F/A_B$, where σ_{MCS}(beam) (which includes the beam angular dispersion) is that measured for the $Z=57$ beam. The latter is found to be 597 MeV/c. With the resulting σ value for each ΔZ_F bin we fit the p_x distribution $f(p_x,p_B)$ by varying p_B and so obtain a value of p_B for each ΔZ_F bin. We also use the LR value of σ_0 as possibly a more realistic description for nuclei.

Fits were obtained by making two different assumptions for the fragment charge to mass conversion: (a) using the most stable nuclei, and (b) using the beam A/Z. Figure 7 shows fits to $f(p_x)$ for case (a) for a mean $A_F=133$, 112, and 70. A similar quality of fits is found for case (b). Table III and Fig. 8 show the fit values of p_B for the five Z_F bins. The χ^2 values are fairly close to unity. It is seen that, within the uncertainties in p_B ($\simeq\pm130$ MeV/c), the extracted values for p_B are fairly independent of the assumed charge to mass conversion. For the Goldhaber model the values for p_B average to about 850 MeV/c in the region for $70<A_F<116$. For the region between 126 and 135, it decreases to about 500 MeV/c. Note that these values are lower by 5 and 25%, respectively, than those reported earlier [28] and supersede them. (It was found that the fitting algorithm used earlier was in error.) As expected, using the LR value of σ_0 results in larger values of p_B. Coulomb forces will give

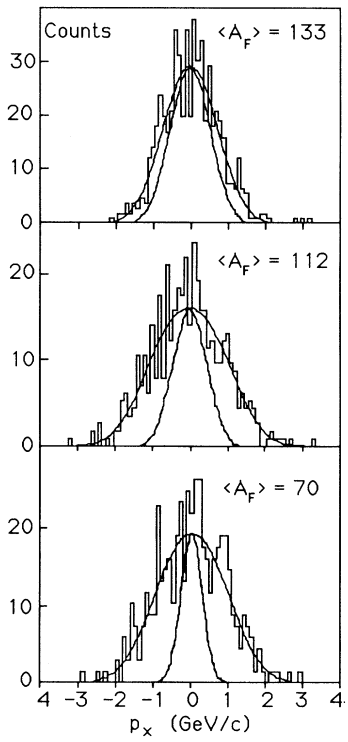

FIG. 7. Measured transverse momentum (p_x) distributions and best fits for La on C at 1.2 GeV/nucleon for mean $A_F=133$, 112, and 70. The cases plotted correspond to assuming these A_F to be the most stable nuclei. The inside curves are the corresponding multiple Coulomb scattering contributions.

TABLE III. Transverse bounce-off momenta p_B extracted for various fragment charge ranges. The Goldhaber model was used for σ_0.

Z_F range	Mean A_F	p_B (MeV/c)	Reduced χ^2	Deg. of freedom
		(a) Most stable		
27–36	70	722±142	0.8	46
37–44	94	794±132	0.9	51
45–50	112	837±125	0.8	49
51–54	126	475±135	1.2	49
55–56	133	403±127	1.2	41
		(b) Beam A/Z		
27–36	77	997±138	1.1	48
37–44	99	904±129	1.0	54
45–50	116	820±123	0.9	52
51–54	128	492±129	1.2	50
55–56	135	457±121	1.1	45

rise to a collective p_T(Coul). This can be estimated using relativistic electrodynamics [47]. A simple two-stage model based on the AA model yields $p_T(\text{Coul}) \simeq 300$ MeV/c for $Z_F = 37$.

The mechanism producing the additional p_T of the nuclear fragment can very likely be viewed as being collective in nature. Collective phenomena such as shock waves in relativistic nuclear collisions are very important in that they should allow one to study extreme conditions of nuclear matter. Early on, it was predicted [48] that these would occur, and that evidence would be the observation of collective sidewards flow of matter, e.g., nucleons. In fact, indications of such flow were present in early emulsion data [49]. However, convincing evidence of flow and bounce-off of light particles (mainly nucleons) came first from 4π electronic detectors at the Bevalac [50,51]. Later, our measurements [27,28] of the large transverse momenta of heavy projectile fragments provided direct evidence of bounce-off of the heavy spectator

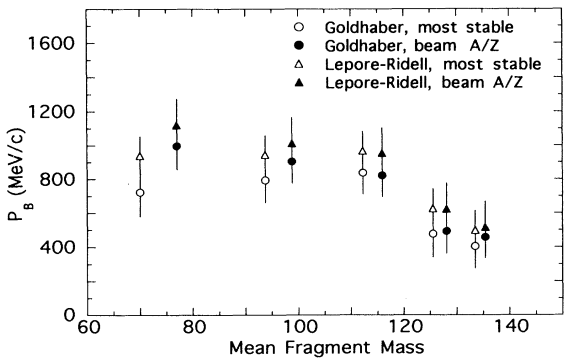

FIG. 8. Extracted values of p_B for La on C at 1.2 GeV/nucleon corresponding to the two assumed fragment charge to mass conversions (see text), and with the contribution due to the effects of internal nucleon momenta corrected as described in the text using the Goldhaber (circles) and Lepore-Riddell prescriptions (triangles).

fragments. Large p_T of lighter fragments up to $Z \simeq 10$ were also measured in 200A MeV Au+Au [52]. Thus, there is a good evidence that the basic assumptions of the hydrodynamic model (short mean free path, rapid local thermalization) are fairly well satisfied.

From a microscopic perspective, one expects that nucleons from the hot overlap or participant region (multiple) scatter from each other and some scatter into the colder spectator fragments where some or all of their energy is absorbed. In this way energy and momentum are transferred to the projectile fragment. Hüfner *et al.* [14] proposed such a final-state-interaction model to account for energy deposition in the fragment by the participant nucleons. Oliveira *et al.* [16] termed this frictional or final-state-interaction energy and adapted this model to introduce additional energy into the abrasion fragments. For nucleon-nucleon scattering at these energies the cross section $d\sigma/dt$ is forward peaked towards small four-momentum transfer, t [53]. Thus, in the laboratory frame one struck nucleon recoils at angles near 90° while the other is changed little in direction or energy. In collisions along the participant-spectator interface, up to nearly 50% of the recoil nucleons can be directed towards the "spectator" projectile fragment, and so can transfer energy and momentum to this projectile abrasion fragment (or prefragment) which deexcites to become the detected projectile fragment (PF).

As shown in Ref. [28], from the data on $d\sigma/dt$ [53] one can calculate the average $\langle t \rangle \simeq 400$ MeV/c $= \mathbf{q}$ (three-momentum) for elastic scattering. The $\mathbf{q}(\theta)$ distribution in the projectile frame peaks near $\theta = 75°$. ($\theta = 0°$ is along the target direction in the projectile frame.) Thus, stopping the recoil nucleon in the PF transfers up to an average of $\simeq 400$ MeV/c in the transverse and $\simeq 100$ MeV/c in the longitudinal direction. If several nucleons stop or transfer a large fraction of their momentum to the PF the latter will receive a collective bounce.

A complete calculation of the momentum transferred to the PF when the C (target) nucleus passes through the La nucleus must include multiple-scattering, mean-field, and other effects. A simple estimate can be made using the energy transfer model of Refs. [14,16]. In the latter it is assumed that as the recoiling nucleon advances through the PF it loses energy by further N-N collisions. The deposited energy is assumed to be $dE = -\alpha E\, dx/\lambda$, where $\alpha = 0.25$ is the fraction of energy lost per collision, and $\lambda(mfp) = (\rho\sigma_{NN})^{-1}$. We assume $\rho = 0.16$ fm^{-3} and that $\sigma_{NN} \simeq (550/E)$ fm^2 is a good approximation for $50 \leq E \leq 150$ MeV.

With the above model the average energy deposited per recoiling nucleon by a PF of $A = 64$ is $\simeq 40$ MeV. The corresponding average momentum deposited is $\simeq 300$ MeV/c (at a mean angle of $\bar{\theta} \cong 75°$). The azimuth, ϕ, of $\mathbf{q}$ varies from near zero to near π so the average $\langle q_x \rangle_\phi$ is $2q/\pi$ or $\simeq 200$ MeV/c. Thus, in a single event one needs only three or four nucleons from the participant region to recoil into the PF to produce the additional p_x required to explain the measured p_x distributions and the additional p_B. These nucleons will also each contribute towards slowing down the PF in the laboratory frame.

Recent calculations [54] indicate that the transverse flow of light ($Z \geq 2$) particles should be a more accurate indication of the reaction plane azimuth than that of nucleons. As mentioned above, the recent measurement [52] of light particles ($3 \leq Z \leq 10$) from 200 MeV Au+Au collisions exhibit stronger flow effects than nucleons. If, as we believe, the extra p_B reflects collision dynamics then it may be possible to use measurements of the PF momentum (or summed momenta) to determine the azimuth of the reaction plane. This determination would apply to noncentral collisions which are a large fraction of the total reaction cross section. According to the abrasion-ablation model, the PF mass provides a measure of the impact parameter, b. Thus, measurements of heavy PF in many cases may be one of the easiest and best ways of determining the vector impact parameter **b**. If the collision geometry can in some cases be well determined then the theoretical models can be applied to these selected collisions without so much averaging over b and over the azimuth of the reaction plane. Calculations [55] show that impact parameter averaging distorts the measurement of liquid-vapor-type phase transitions, and that for such measurements it is crucial to know the geometry of each collision. Similar conclusions apply to the study of nuclear flow and the extraction of information regarding the nuclear equation of state.

In summary, we have measured the charge and transverse momentum distributions of heavy projectile fragments produced in 1.2 GeV per nucleon ^{139}La+C collisions. The most interesting findings are that the transverse momenta are larger than predicted on the basis of internal nuclear momenta. It also appears that the σ_0 parameter has a dependence on fragment mass while the models predict it to be constant. The momentum distributions can be fit by folding in an extra p_T which we call p_B(bounce). Thus, these measurements of the heavy projectile fragment transverse momenta indicate that fragmentation may contain more physics than initially believed. The p_T measurements may also call into question the target independence and isotropy (in the projectile frame) of the momentum distributions predicted by the present, relatively simple, theories. In addition, if a large part of p_T of the heavy fragments reflects collision dynamics, then it may be possible, at least for peripheral collisions, to use $\mathbf{p}_T$ of the heavy fragments to establish the azimuth of the reaction plane (more accurately than the flow of nucleons), while the mass may provide a measure of b.

ACKNOWLEDGMENTS

We are grateful to F. Bieser, I. Flores, and J. Porter at LBL and to E. Barasch, C. Casteneda, J. Chance, J. Drummond, and M. Webb at UCD for willing and essential assistance. We acknowledge the support of the National Science Foundation under Grant Nos. PHY84-19380 and PHY87-22008, the Department of Energy under Contract No. DE-AC03-76SF0098, NASA under Grant No. NGR 05-003-513, and the Gesellschaft für Schwerionenforschung, Darmstadt, FRG. Three of us (C.E.T., B.C.M., and J.C.Y.) acknowledge support through Associated Western Universities.

[1] H. H. Heckman, D. E. Greiner, P. J. Lindstrom, and F. S. Bieser, Phys. Rev. Lett. **28**, 926 (1972).
[2] D. E. Greiner, P. J. Lindstrom, H. H. Heckman, B. Cork, and F. S. Bieser, Phys. Rev. Lett. **35**, 152 (1975).
[3] P. J. Lindstrom, D. E. Greiner, H. H. Heckman, Bruce Cork, and F. S. Bieser, LBL Report No. LBL-3650, 1975.
[4] L. M. Anderson, Ph.D. thesis, Lawrence Berkeley Laboratory Report No. LBL-6769, 1977 (unpublished); L. Anderson, W. Brückner, E. Moeller, S. Nagamiya, S. Nissin-Meyer, L. Schroeder, G. Shapiro, and H. Steiner, Phys. Rev. C **28**, 1224 (1983).
[5] J. Papp, Ph.D. thesis, LBL Report No. LBL-3633, 1975 (unpublished); J. Papp, J. Jaros, L. Schroeder, J. Staples, H. Steiner, A. Wagner, and J. Wiss, Phys. Rev. Lett. **34**, 601 (1975).
[6] H. H. Heckman, D. E. Greiner, P. J. Lindstrom, and H. Shwe, Phys. Rev. C **17**, 1735 (1978).
[7] A. S. Goldhaber, Phys. Lett. **53B**, 306 (1974); H. Feshbach and K. Huang, *ibid.* **47B**, 300 (1973).
[8] J. V. Lepore and R. J. Riddell, Jr., LBL Report No. LBL-3086, 1974 (unpublished).
[9] D. L. Olson, B. L. Berman, D. E. Greiner, H. H. Heckman, P. J. Lindstrom, and H. J. Crawford, Phys. Rev. C **28**, 1602 (1983).
[10] D. L. Olson, B. L. Berman, D. E. Greiner, H. H. Heckman, P. J. Lindstrom, G. D. Westfall, and H. J. Crawford, Phys. Rev. C **24**, 1529 (1981).
[11] Y. P. Viyogi *et al.*, Phys. Rev. Lett. **42**, 33 (1979).
[12] E. J. Moniz *et al.*, Phys. Rev. Lett. **26**, 445 (1971).
[13] J. D. Bowman, W. J. Swiatecki, and C. F. Tsang, LBL Report No. LBL-2908, 1973 (unpublished).
[14] J. Hüfner, K. Schäfer, and B. Schürmann, Phys. Rev. C **12**, 1888 (1975).
[15] J. Hüfner, C. Sanders, and G. Wolschin, Phys. Lett. **73B**, 306 (1974).
[16] L. F. Oliveira, R. Donangelo, and J. O. Rasmussen, Phys. Rev. C **19**, 826 (1979).
[17] G. D. Westfall, L. W. Wilson, P. J. Lindstrom, H. J. Crawford, D. E. Greiner, and H. H. Heckman, Phys. Rev. C **19**, 1309 (1979).
[18] H. H. Heckman and P. J. Lindstrom, Phys. Rev. Lett. **37**, 56 (1976).
[19] J.-J. Gaimard and K.-H. Schmidt, GSI Report No. GSI-91-14, 1991; Nucl. Phys. **A531**, 709 (1991).
[20] W. R. Binns *et al.*, Phys. Rev. C **39**, 1785 (1989).
[21] R. Silberberg, C. H. Tsao, and J. R. Letaw, Astrophys. J. Suppl. **58**, 873 (1985), and references therein.
[22] W. R. Binns *et al.*, Phys. Rev. C **36**, 1870 (1987).
[23] J. R. Cummings *et al.*, Phys. Rev. C **42**, 2508 (1990).
[24] J. R. Cummings *et al.*, Phys. Rev. C **42**, 2530 (1990).
[25] W. R. Webber, J. C. Kish, and D. A. Schrier, Phys. Rev. C **41**, 520 (1990); **41**, 533 (1990); **41**, 566 (1990).
[26] W. B. Christie *et al.*, Nucl. Instrum. Methods A **255**, 466 (1987), and references therein.

[27] F. P. Brady *et al.*, in *Hadronic Probes and Nuclear Interactions (Physical Science Center at Arizona State University, Tempe, Arizona),* Proceedings of the International Conference on Hadronic Probes and Nuclear Interactions, AIP Conf. Proc. No. 133, edited by J. R. Comfort, W. R. Gibbs, and B. G. Richie (AIP, New York, 1985).
[28] F. P. Brady *et al.*, Phys. Rev. Lett. **60**, 1699 (1988).
[29] D. E. Greiner, LBL Report No. LBL-18728, 1984 (unpublished); J. Engalage *et al.*, Nucl. Instrum. Methods A **297**, 431 (1989).
[30] R. C. Jared, D. A. Landis, and F. S. Goulding, IEEE Trans. Nucl. Sci. **NS-29**, 57 (1982); D. A. Landis, R. S. Adachi, N. W. Madden, and F. S. Goulding, *ibid.* **NS-29**, 62 (1982).
[31] R. C. Jared, Z. Y. Fujita, H. G. Jackson, S. B. Sidman, and F. S. Goulding, IEEE Trans. Nucl. Sci. **NS-29**, 282 (1982); S. Sidman, S. Olson, and R. Jared, Lawrence Berkeley Laboratory Report No. LBL-15676 (1982).
[32] L. Landau, J. Exp. Phys. (USSR) **8**, 201 (1944).
[33] P. V. Vavilov, Zh. Eksp. Teor. Fiz. **32**, 920 (1957) [Sov. Phys. JETP **5**, 749 (1957)].
[34] G. D. Badhwar, Nucl. Instrum. Methods **109**, 119 (1973).
[35] J. H. Adams, Jr., R. Silverberg, and G. D. Badhwar, Nucl. Instrum. Methods **124**, 551 (1975).
[36] W. J. F. Müller *et al.*, Lawrence Berkeley Laboratory Report No. LBL-24580 (1988).
[37] H. L. Bradt and B. Peters, Phys. Rev. **77**, 54 (1950).
[38] T. F. Cleghorn, P. S. Freier, and C. J. Waddington, Can. J. Phys. **46**, 6 (1968).
[39] P. J. Karol, Phys. Rev. C **11**, 1203 (1975).
[40] M. P. Kertzman, J. Klarmann, B. J. Newport, E. C. Stone, C. J. Waddington, W. R. Binns, T. L. Garrard, and M. H. Israel, Int. Cosmic Ray Conf. **19**, 95 (1985).
[41] D. J. Morrissey, W. R. Marsh, R. J. Otto, W. Loveland, and G. T. Seaborg, Phys. Rev. C **18**, 1267 (1978).
[42] W. J. Swiatecki, LBL report, 1976 (unpublished).
[43] Y. Eisenberg, Phys. Rev. **96**, 1378 (1954).
[44] X. Campi and J. Hüfner, Phys. Rev. C **24**, 2199 (1981).
[45] W. J. F. Müller *et al.* (unpublished).
[46] G. F. Bertsch, Phys. Rev. Lett. **46**, 472 (1981).
[47] J. D. Jackson, *Classical Electrodynamics* (Wiley, New York, 1962), p. 431: $p_T(\text{Coul})=ZZ'e^2/bv$.
[48] W. Scheid, H. Müller, and W. Greiner, Phys. Rev. Lett. **21**, 741 (1974).
[49] A. G. Baumgardt *et al.*, Z. Phys. A **273**, 359 (1975).
[50] H. A. Gustafson *et al.*, Phys. Rev. Lett. **52**, 1590 (1984).
[51] R. E. Renfordt *et al.*, Phys. Rev. Lett. **53**, 763 (1984).
[52] K. G. R. Doss *et al.*, Phys. Rev. Lett. **59**, 2720 (1987).
[53] O. Bernary, L. R. Price, and G. Alexander, LRL Report No. UCRL-20000, 1970 (unpublished).
[54] G. Fai, Wei-ming Zhang, and M. Gyulassy, Phys. Rev. C **36**, 597 (1987).
[55] G. Peilert, A. Rosenhauer, H. Stöcker, W. Greiner, and J. Aichelin, ITP Report No. UFTP 202/1987, 1987; Mod. Phys. Lett. **3**, 459 (1988).